Analysis of atomic and ion debris features of laser-produced Sn and Li plasmas

R. W. Coons,[a] S. S. Harilal, D. Campos, and A. Hassanein
School of Nuclear Engineering and Center for Materials Under Extreme Environment, Purdue University, West Lafayette, Indiana 47907, USA

(Received 3 May 2010; accepted 5 August 2010; published online 28 September 2010)

Tin and lithium plasmas emit efficiently in the in-band region (13.5 nm with 2% bandwidth) necessary for extreme ultraviolet (EUV) lithography. We have made a detailed comparison of the atomic and ionic debris, as well as the emission features of Sn and Li plasmas under identical experimental conditions. Planar slabs of pure Sn and Li were irradiated with 1064 nm, 9 ns neodymium-doped yttrium aluminum garnet laser pulses for producing plasmas. A suite of diagnostics were used to analyze the emission and debris features, including optical emission spectroscopy (OES), a Faraday cup, an EUV pinhole camera, the absolute measurement of EUV conversion efficiency (CE), etc. Our results show that Sn plasmas provide a CE nearly twice that of Li. However, the kinetic energies of Sn ions are considerably higher, though with a lower flux. OES studies have showed that the kinetic energies of neutral species are substantially lower compared to that of the charged particle species. © *2010 American Institute of Physics*. [doi:10.1063/1.3486209]

I. INTRODUCTION

The optical lithographic processes for semiconductor manufacturing are approaching their theoretical limits.[1,2] The fabrication of smaller features onto substrates depends on a new manufacturing technique; extreme ultraviolet lithography (EUVL) is to be employed.[3,4] The advent of multilayered mirrors (MLMs), made from Mo and Si which can reflect nearly 68% of 13.5 nm light within a 2% bandwidth, are the first optics capable of working in this regime, since the quartz lenses currently used to focus patterns into the photoresist are absorbers of EUV radiation. The leading candidates for the 13.5 nm light sources are laser-produced plasmas (LPP) (Refs. 3 and 4) and discharge-produced plasmas (DPP).[3–7] LPPs have several advantages over DPPs, such as power scalability, minimal heat loads, and a larger angle of collection.[4] Much research has been conducted on generating LPPs from a number of different target materials, including Sn,[8,9] Xe,[10] and Li.[6,11] The essential requirements of a LPP source for EUVL are a high conversion efficiency (CE; conversion from laser energy to 13.5 nm with 2% bandwidth) with minimum debris generation. Among the targets analyzed, Li and Sn provided highest CE from laser energy to 13.5 nm radiation.

The EUV CE from a LPP plasma strongly depends on various laser (wavelength,[12] pulse width,[13] spot size,[14] power density,[15,16] etc.) and target (mass density,[15] target geometry,[16] etc.) parameters. The mass-limited target provides less debris compared to full density targets.[9] However, the spectroscopic and debris analysis of pure materials are necessary to serve as a benchmark in order to ensure that the mass-limited targets are not mass-reduced targets, and offer a comparable EUV CE as a pure target. Previous studies have clearly showed that Sn plasmas are more efficient in EUV generation in the in-band region compared to Li or Xe plasmas.[17,18] Apart from CE, the cleanness of the LPP sources is extremely important for their use in EUVL. The LPP emits debris in the form of energetic ions, atoms, and molten droplets, which are difficult to control.[9,19–22] This ablated target material vapor-deposits itself on various components within a direct line-of-sight of the plasma, including the surface of the MLM, which causes degradation in mirror reflectivity. Additional reflectivity losses are a result of ion-induced sputtering damage to the mirror itself. Previous studies showed that along with fast moving ions, Sn neutrals also contribute a significant reduction in MLM reflectivity.[23] Several schemes for mitigating the ion and atom debris have been proposed,[9,19,24,25] although they cannot completely mitigate the additional damage from neutrally-charged debris. Because of their negative effects, ion and neutral debris must be further characterized, so that effective debris mitigation schemes can be implemented.

The EUV CE, spectral features, and debris analysis of Sn and Li plasmas are extensively documented in the literature.[11,14,17,18,26,27] However, the reported values of CE for Sn and Li plasmas varied from 2%–5% (Ref. 26 and 28) and 1%–2%,[11,26] respectively. The large variation in CE is mainly attributed to changes in experimental parameters. This is somewhat surprising; for example, the reported values for Sn or Li CE using 1064 nm excitation varied from group to group by nearly a factor of 2. This indicates that it is necessary to have a detailed investigation of EUV emission features, along with debris analysis, of Sn and Li plasmas under identical experimental conditions. In this paper, we compared the EUV emission features, as well ion and atom debris, emanating from two efficient LPP target sources (Li and Sn) under identical experimental conditions. For producing plasma, 9 ns pulses from a neodymium-doped yttrium aluminum garnet (Nd:YAG) laser were utilized. We also investigated the effect of laser spot size and laser power density on the CE and the EUV spectral features of both Li and

[a]Electronic mail: rwcoons@purdue.edu.

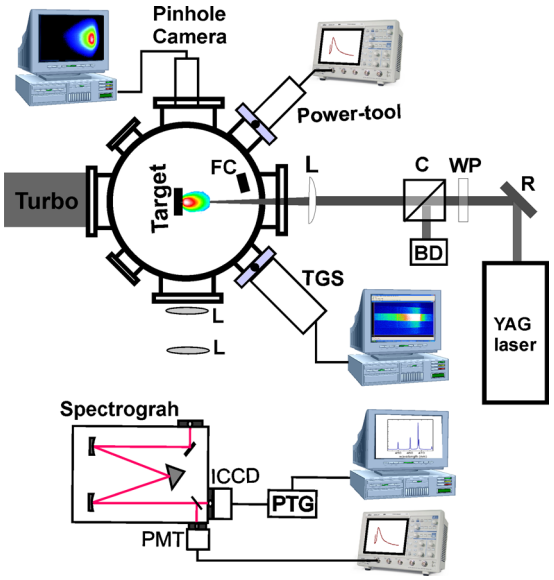

FIG. 1. (Color online) Schematic of experimental setup. Optical components include a polarizing cube (C), a half-wave plate (WP), lens (L), reflector (R), and beam dumps (BD). Diagnostic components include a FC; PTG; ICCD camera; PMT; and transmission grating spectrograph (TGS).

Sn plasmas. The ion fluence and ion energies for each material were measured, along with images and emission spectra of their plasmas. Optical emission spectroscopy (OES) was utilized to investigate the atomic emissions from these plasmas.

II. EXPERIMENTAL SETUP

A schematic of the experimental set up is given in Fig. 1. For producing plasmas, 1064 nm, 9 ns [full width half maximum (FWHM)] pulses from a Nd:YAG laser were used. The laser was attenuated using a combination of a half-wave plate and a polarizing cube. Planar slabs of pure Sn and Li were mounted to a servo-motor controlled XYZ translation stage inside a stainless steel high-vacuum chamber. The chamber is evacuated with a turbomolecular pump to a pressure lower than 10^{-6} Torr. A 40 mm planoconvex focusing lens was mounted to a translation stage with a micrometer actuator, allowing for the tunability of the laser spot size. The target was translated between shots to refresh the target surface, and to mitigate the effects of target cratering. This new surface was exposed to a low energy "cleaning pulse" to ablate the oxide layers of the target before each measurement. The planar target geometry emits EUV radiation through a solid angle of 2π steradians.

The CE of the incident pulse energy to 13.5 nm radiation was measured with an EUV power tool, consisting of two Zr filters and a Mo/Si MLM to reflect the incoming plasma light into an absolutely calibrated photodiode. The photodiode signal is then displayed and recorded on an oscilloscope. The emission spectra of Li and Sn plasmas were recorded using a transmission grating spectrometer (TGS). The TGS utilizes a silicon nitride diffraction grating with a 10,000 lines/mm resolution. The spectra were then recorded with a EUV sensitive charge coupled device (CCD) camera (Princeton Instruments PIXIS) in a time-integrated manner. EUV images of the plasma were obtained by mounting a 50 μm pinhole at the end of a 49.2 cm tube, placed 51 mm from the target point, creating a simple pinhole camera with a magnification of 11. The pinhole camera employs a Zr filter which filters radiation in the wavelength range 7–15 nm.

The fluence and kinetic energy (KE)of the plasma ions were measured with a Faraday cup (FC) mounted inside the chamber at a distance 17 cm from the target point, at a 12° angle from the plane of the beam. The FC was biased with a dc power supply to the optimized potential difference of −31 V. The ion current was measured by acquiring the voltage signal across a load resistor by 350 MHz digital phosphor oscilloscope (Lecroy Model WJ334).

We also utilized OES to characterize neutrals from Sn and Li plasma. The light emitted from the luminous plasma was transmitted though a quartz window mounted orthogonally to the direction of plume expansion. An optical system was used to image the plasma plume onto the entrance slit of a 0.5 m Czerny–Turner spectrograph (Acton, Spectrapro SP2500i). The spectrograph was equipped with three gratings of 150 grooves/mm, 600 grooves/mm, and 1800 grooves/mm, with effective dispersions of 12.8 nm/mm, 3.1 nm/mm, and 0.75 nm/mm, respectively. One of the exit ports of the spectrograph was coupled to an intensified CCD (ICCD, PI MAX) and the other exit port was coupled to a photomultiplier tube (PMT, Hamamatsu R928, rise time 2.2 ns). A diverter mirror was used for switching from the PMT to the ICCD or vice versa. A programmable timing generator (PTG) was used to control the delay time between the laser pulse and the detector system, with an overall temporal resolution of 1 ns. The spectrograph and detectors are sensitive to a spectral window of 250–800 nm. For recording the temporal profiles of a particular species in the plume, the specific lines were selected by tuning the grating and imaging onto the slit of the PMT. The output of the PMT was directly coupled to a digital phosphor oscilloscope (Lecroy 350 MHz Model WJ334). This setup provides the delay as well as the decay of the emission of a constituent species within the plasma, which are very important parameters related to the evolution of laser-ablated materials in a direction normal to the target surface.

III. RESULTS AND DISCUSSION

A. EUV emission features

The dependence of in-band CE for three spot sizes is evaluated at many different laser intensities for Sn and Li, as shown in Fig. 2. The EUV measurements show that CE is highly dependent on target material, as well as beam intensity and laser spot size. Our measurements showed that Sn plasma provides a higher CE, reaching peak levels of 2%, as opposed to the Li peak of 1%, which are consistent with previously reported values.[11,13] The optimal CE achieved is irrespective of the spot sizes used, which was found to be consistent with recent report of spot size dependence on Sn plasma CE.[14] The CE remains constant irrespective of the spot size due to the balance between the laser energy losses due to the lateral expansion of the plasma and the reabsorption of the EUV light.[14] Visible emission images employing

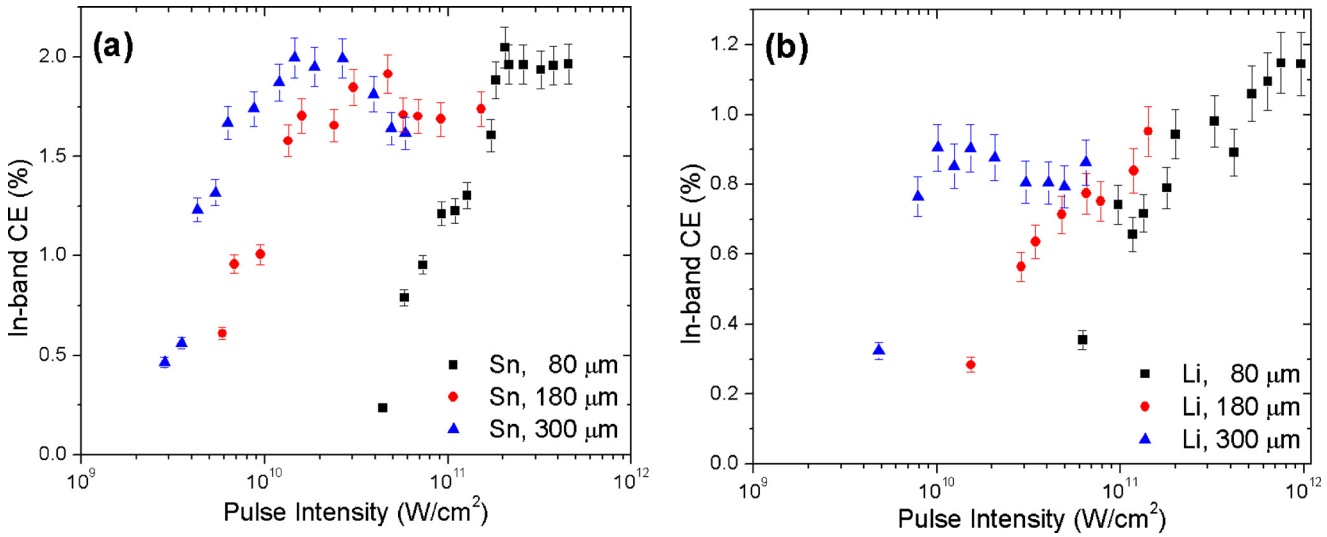

FIG. 2. (Color online) The dependence of CE on laser intensity is given for various spot sizes for Sn (a) and Li (b) plasma.

fast imaging clearly showed that with a smaller spot size the plasma expansion is nearly spherical, while with a larger spot size plasma expands cylindrically.[29]

A smaller spot size requires a higher intensity to reach the same CE as a large spot size, as seen in Fig. 2. For obtaining the highest CE, ideal plasma temperatures and densities should be created for the longest possible period of time with the maximum size. The changes in the spot size will affect the nature of the hydrodynamic expansion and confinement of the plasma.[29] The magnitude of the plasma temperature is provided by a balance between incoming and escaping energy (laser absorption, radiation energy loss, plasma expansion, etc.). The present results are consistent with recent modeling studies, which predicted the requirement of a higher laser intensity for a smaller spot size.[16] In the case of larger laser spots, lower laser irradiances are needed for efficient EUV production because of the plasma opacity, and the smaller laser spots create the opposite effect.[16] Hence, the hydrodynamic confinement plays a role in the right shift in CE maxima with smaller spot sizes.

The saturation or reduction in the CE of Sn plasma at higher intensities after reaching the optimal CE could be due to opacity effects. It is well known that the plasma from a solid Sn target is optically thick to 13.5 nm light.[30] However, we noticed CE saturation in Li plasmas as well, especially at larger spot sizes, where the plasma evidently provides a slightly lower CE. For example, Fig. 2(b) shows the obtained maximum CE with a 300 μm spot is 0.9%, while it increased to 1.1% with a 80 μm spot size plasma.

Spectra of both materials were recorded with laser pulses of increasing intensity, with a constant spot size of 80 μm, and are given in Fig. 3. The EUV emission from the Sn plasma showed a broadband emission constituted by several ionic stages [an unresolved transition array (UTA)].[12] The UTA emission is concentrated around 13.5 nm, with a narrow band gap of 5–10 eV arising from the $4p^64d^n - 4p^54d^{n+1} + 4p^64d^{n-1}4f$ transitions of various Sn ions, ranging from Sn^{6+} to Sn^{14+}, with occupancy in transition levels from the range of $n=2$ to $n=8$. The main contributors of emission in the in-band region are Sn^{9+}–Sn^{13+} ions. At high

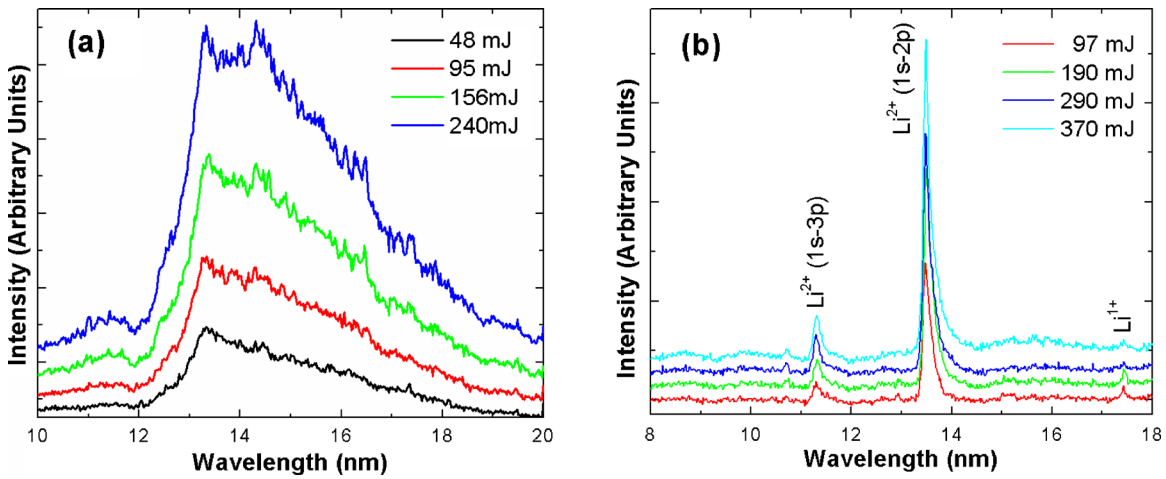

FIG. 3. (Color online) EUV spectral emission features of Sn (a) and Li (b) plasmas. A transmission grating spectrograph with a resolution of $100(\lambda/\Delta\lambda)$ is used for recording the spectra.

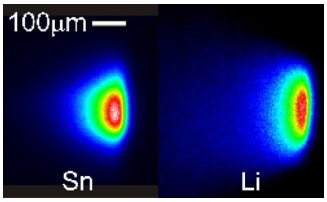

FIG. 4. (Color online) Images of Sn and Li plasmas. False-color has been added to the images to show relative intensities. The Li plasma image is a multiple exposure of four pulses and the Sn plasma image is of a single pulse.

laser energies, a spectral dip at the peak of the UTA is evident, which is mainly due to opacity effects causing self-absorption.[14] An enhancement in intensity is also noted at the higher wavelength side of the UTA with increasing laser intensity. These enhancements are due to recombination effects, where ionized Sn atoms collide with free electrons in the plasma, repopulating the Sn^{8+}–Sn^{10+} levels, where they strongly radiate in the out-of-band region.[31] This indicates that more out-of-band emission will be present with increasing laser energies. Out-of-band emission will then be accompanied by an increase in debris, and any system operating in this region would require an effective mitigation system.[32] Li plasmas possess a discrete line structure, the Li^{2+} $1s-2p$ transition (Lyman-α) at 13.5 nm, as seen in Fig. 3(b), which lies completely within the 2% bandwidth of the Mo/Si MLM. This spectral feature became more intense with increasing laser intensity, but the feature's shape remained unchanged. The TGS used in these studies only had a resolution ($\lambda/\Delta\lambda$) of $\sim$100, which is inadequate to resolve the finer spectral details.

The plume images obtained with a pinhole camera are shown in Fig. 4, where it was observed that the EUV emission from the Li plasma was significantly dimmer than those obtained from a Sn plasma at a given laser intensity. While the Sn plasma was bright enough to be imaged easily, imaging the Li plasma required taking a multiple exposure of four separate plasmas. Our pinhole camera integrates a spectral region from 7–15 nm, where the Li emission is entirely due to the Lyman-α line, while the camera captures almost the entire Sn UTA. The aspects ratios were obtained by measuring the drop-off from the image's intensity profile peak to $1/e^2$ of that peak value. The Li plasma had an aspect ratio of 1.22 and the Sn had a ratio of 1.26; so both plasmas have similar aspect ratios, despite having apparently different shapes.

B. FC ion analysis

In addition to radiating the 13.5 nm in-band light, a LPP will also release debris in the forms of energetic ions, neutral particles, molten droplets ejected from the ablated target, and out-of-band emission.[19] Ionized and neutral particle flux causes the sputtering and implantation of the debris species into the MLM coating, lowering its reflectivity.[23] In order for the EUV lithography to be a commercially viable manufacturing technique, the lifetime of the MLMs must last a long time. Several mitigation schemes have been devised to improve the lifetime of the MLMs, using magnetic fields,[9,25,33] a gas curtain,[19,24] low energy prepulses,[8] and mass-limited targets.[15,28]

FCs are one of the simplest methods for analyzing ions from LPPs. However, they provide an integrated ion signal containing all charge states, and space charge effects could distort the FC signal.[34] Nevertheless, it is a very useful tool for obtaining the integrated ion flux, the velocity of the ions, and hence, the KE distribution. We characterized and compared the ion emissions from Sn and Li plasmas using a FC. The FC was positioned at 17 cm from the plasma at an angle of 12° with respect to target normal for all measurements. Typical ion profiles obtained from Sn and Li plasma are given in Fig. 5, along with their KE profiles. The laser intensity used for these measurements was 2×10^{11} W/cm^2, with a spot size of 80 μm. The ion time-of-flight (TOF) profile is represented by a sharp prompt peak, followed by a broad slower peak. The fast prompt peak in the ion signal is caused by the photoelectric effect and can be used as a time marker. It is very evident from the figure that Li ions possess a narrower kinetic profile compared to Sn ions. The measured peak expansion velocities are $4.2\pm0.2\times10^6$ cm/s for Sn ions and $1.4\pm0.2\times10^7$ cm/s for Li ions. However, due to

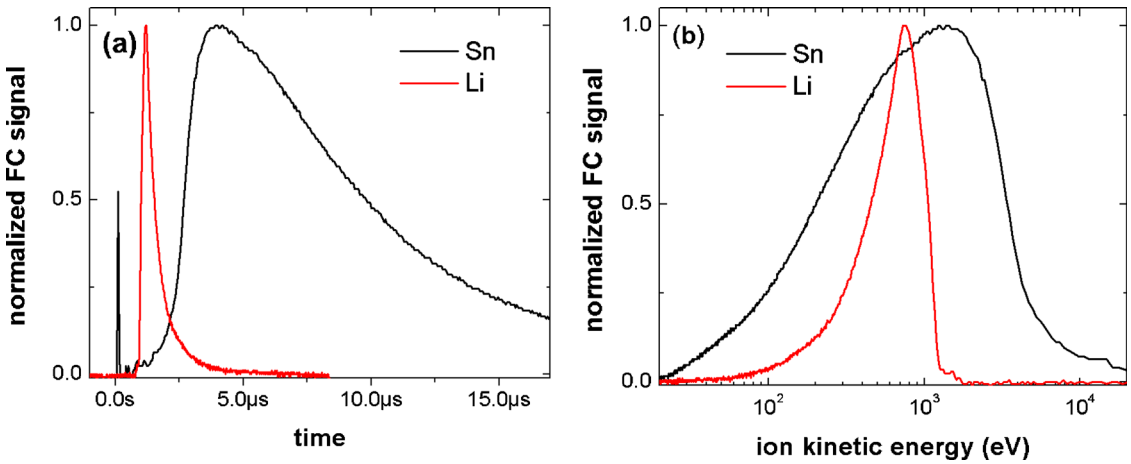

FIG. 5. (Color online) Typical ion profiles (a) recorded with a FC are given for Sn and Li plasma. For these measurements the FC is positioned at 17 cm from the target at an angle 12°. The laser intensity used in this measurement is 2×10^{11} W/cm^2. The kinetic distribution obtained from the TOF ion signal is given in (b).

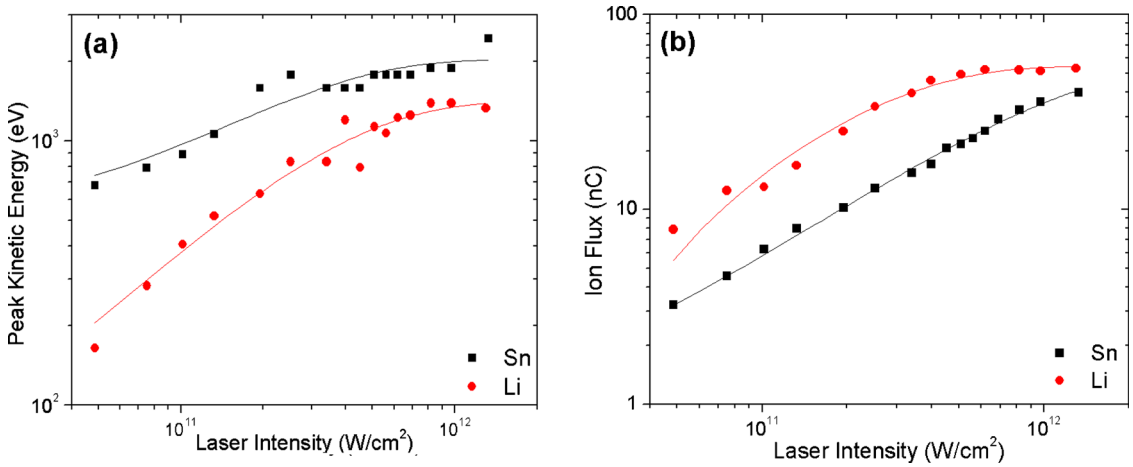

FIG. 6. (Color online) The estimated maximum probable KEs of Sn and Li plasma (a) and ion flux (b) as a function of laser intensity are given. The smooth curves in the figures represent a best fit obtained with an exponentially saturating curve fitting.

their lower mass, the KE of the Li ions is considerably lower compared to the Sn ions. The KE FWHM spread of Sn ions was found to be 5× greater compared to Li ions at the laser intensity of 2×10^{11} W/cm^2. Under these intensity conditions, the average charge state $\langle Z\rangle$ of Sn plasma[35] be ≥11, while for Li, ≥2. However, the plasma ions undergo recombination during their flight to the detector. The major contributor to recombination during the adiabatic expansion phase was three-body recombination.

The maximum probable KEs, as well the ion flux of Sn and Li plasmas, depend on laser intensities. Figure 6 shows the estimated maximum probable KE and ion flux for Sn and Li plasma at various laser intensities. For both Li and Sn plasmas, the maximum probable KE, as well ion fluence, showed an exponentially saturating trend. The saturation in KEs and ion flux at higher laser intensities could be due to plasma shielding and/or absorption. Previous studies with identical laser intensities[8] for Sn plasmas clearly showed the plasma could already be at the critical density for the pump beam wavelength. Once the plasma reaches the critical density, the remaining part of the laser pulse will interact with the plasma rather than the target material, which effectively limits the ion flux. However, it should be mentioned that space charge effects could distort the FC signal, leading to errors in the estimation of the peak KEs. Janmohamed *et al.*[34] reported a detailed description of the influence of space charge effects on the ion signal and they found that electrons play an important role in the space charge distortion phenomena. The saturation of ion KE can also be related to the measurement of the CE, where we also noticed a similar saturation at higher intensities.

Comparing the ion flux and KEs of Sn and Li plasma, one can notice that the peak KEs are always higher for Sn plasma, which could make them more deleterious for MLM mirrors. These results showed that implementing charged particle debris mitigation techniques (electric or magnetic field) is much easier for Li plasma. However, FC studies showed that although they are less energetic, the ion fluence is significantly higher for Li plasma compared to Sn plasma.

C. OES analysis

The debris from LPP includes energetic ions as well as neutral particles. It is known that neutrals are relatively slow moving particles compared to energetic ions,[36] however, controlling ions is much easier by exploiting their charge state.[19,37] Neutrals can also possess high KEs, due to their origin from recombination processes. Little effort has been spent on understanding the evolution of the fast neutrals from Sn and Li plasmas. Typical diagnostic tools employed for understanding the evolution of neutrals in a plume are laser-induced fluorescence[38] and optical TOF (OTOF)-emission spectroscopy.[39,40] OES is one of the simplest, nonintrusive ways to investigate early plasma dynamics, since it uses the intrinsic light emission from the LPP, and does not require external excitation. Spectral details can also be useful for estimating the plasma ionization balance, rate processes, densities, and temperatures.[41] Even though OTOF studies will not provide the number density of the excited neutral species, these studies are extremely useful for understanding how the neutral species evolve, and provide a KE distribution of excited neutral species.

Typical time-integrated optical spectra obtained from Sn and Li plasma are given in Fig. 7. The spectra are obtained with an integrating time of 2 μs. The recorded emission spectra mainly contained singly charged ions and neutrals. The prominent emission lines are marked in the figure. We selected the strongest Sn and Li ions and neutrals lines for OTOF studies. The neutral lines selected are 317.5 nm ($5p^2\ ^3\mathrm{P}-6s\ ^3\mathrm{P}$) and 460.3 nm ($1s^22p-1s^24d$) for Sn and Li plasma. The single ionic lines selected for OTOF are 556 nm ($6d^2\mathrm{D}-6p^2\mathrm{P}_0$) and 468 nm ($1s3d-1s4f$) for Sn and Li plasmas, respectively. For studying the time evolution of excited neutral species, the TOF profiles of selected lines were recorded for distances up to 14 mm.

Typical TOF profiles of Sn and Li neutrals recorded 10 mm from the target are given in Fig. 8. These measurements were made with a laser intensity of 2×10^{11} W/cm^2. The sharp spike observed at earlier times is the prompt signal that is used as a time marker. The temporal emission features are affected by the presence of strong continuum at short dis-

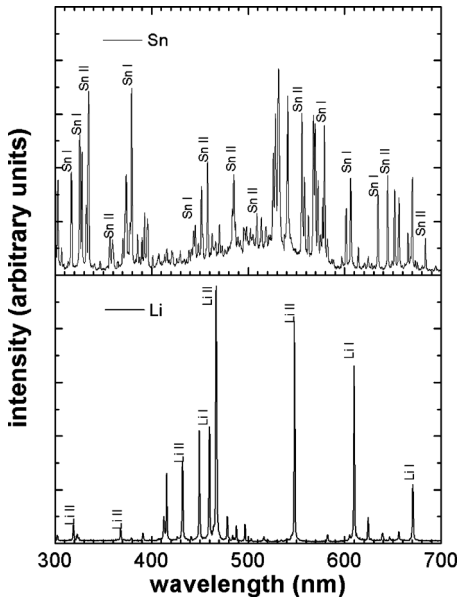

FIG. 7. Time-integrated spectra of Sn and Li plasmas, displaying the strongest lines from both neutral and singly charged states.

tances (≤ 2 mm) and at early times, but at distances >2 mm the continuum emission is considerably reduced and its interference on the TOF profiles is negligible. In order to gain more insight into the kinetic properties of the plume species, a shifted Maxwell–Boltzmann (SMB) distribution was fitted to the TOF profiles to investigate the kinetic properties of the plume. The SMB fitting function is given by

$$f(v) = A\left(\frac{m}{2\pi k}\right)^{3/2} v^3 e^{-m(v-v_0)^2/2kT} dv, \quad (1)$$

where A is a normalization constant, v and v_0 are the velocities of the species and the center-of-mass velocity, T is the translational temperature, k is the Boltzmann constant, and m is the mass of the species. The SMB distribution assumes that the speed distribution has equilibrated after propagating a short distance from the target surface and that the signal is a direct measure of the concentration of the indicated species. As the figure shows, the SMB distribution fits reasonably well with Li and Sn neutral lines.

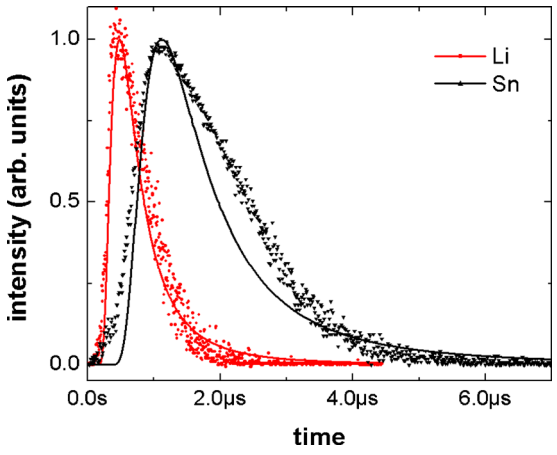

FIG. 8. (Color online) TOF profiles of neutral Sn and Li atoms 10 mm away from the target surface, as determined by the atomic optical emission measured with a PMT. The smooth curves in the plot correspond to SMB fit using Eq. (1).

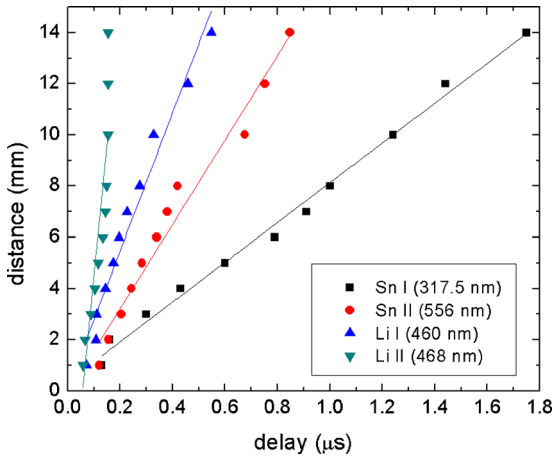

FIG. 9. (Color online) Spatial propagation of neutral and singly-ionized Sn and Li as determined from their optical emission measured with a PMT.

The position-time (R-t) plot obtained from the OTOF studies for neutral and singly-ionized Sn and Li are given in Fig. 9. A linear fit was applied to each species, so that their velocities could be calculated from their slopes. The slopes of the ionized species show that the Sn and Li ions possess velocities of $1.6 \pm 0.1 \times 10^6$ and $1.3 \pm 0.3 \times 10^7$ cm/s which corresponds to KEs of 609 and 158 eV. Though the estimated Li ion expansion velocity from OTOF agrees well with FC measurement values, the Sn ion OTOF velocity was considerably lower than its FC measured value. This can be easily understood by considering the average charge state of Sn and Li plasmas under the laser intensities used in the present studies, and the space charge effects in LPP's. The FC signal of Sn contains a wide range of Sn charge states, while the Li ionic signal is contributed by three ionic stages.

The estimated velocities of Sn and Li neutrals from the R-t plots are $8.5 \pm 0.5 \times 10^5$ and $1.4 \pm 0.2 \times 10^6$ cm/s, and their corresponding KEs are 44 eV and 7 eV, respectively. These values indicate that the KEs of Sn neutrals are more than 6× that of Li. However, the measured energies of neutrals are substantially less compared to ion energies and the implantation of the neutrals in the MLM mirrors can be only at the surface. Hence, the slow moving neutrals are expected to be deposited on the mirror, rather than implanted into it.

The ion profiles, as well as the atomic profiles of a Li plasma were shown to be considerably narrower compared to those of a Sn plasma. This could be due to the Z-dependence of both the mass ablation rate and the recombination rate. The mass ablation rate of the target in a LPP, is given by[42]

$$\dot{m} \approx (3.0 \times 10^3)\left(\frac{I_a}{10^{11}\ \mathrm{W/cm^2}}\right)^{5/9}\left(\frac{\lambda_L}{1\ \mu\mathrm{m}}\right)^{-4/9} \times Z^{3/8}\left(\frac{g}{\mathrm{cm^2\ s}}\right),$$

where I_a is the laser pulse intensity, λ_L is the laser wavelength, and Z is the atomic number. For a 1.064 μm laser pulse with an intensity of 10^{12} W/cm^2, the mass ablation rate was calculated to be 4.55×10^4 g/cm^2 s for Sn and

1.58×10^4 g/cm^2 s for Li. This indicates the mass ablation rate is nearly three times higher for Sn target compared to Li. The three-body recombination rate is related to Z through the equation[43]

$$R_{recomb} = \left(\frac{dn_e}{dt}\right)_{recomb} = -9.2\times10^{-39}\ Z^3 T_e^{-9/2} \ln(\sqrt{Z^2+1}) n_e^2 n_i,$$

where T_e is the electron temperature in eV and n_e and n_i are the electron and ion densities, respectively, given in m^{-3}. EUV-emitting regions of Sn plasmas have average electron temperatures of ~30 eV (Ref. 44) and ~14 eV for Li.[26] The plasma densities were measured from the Stark broadening profiles obtained from two-dimensional OES, the details of which are discussed elsewhere.[44] At a distance of 0.5 mm from the target surface, $\bar{Z}\approx8$ for Sn (Ref. 44) and $\bar{Z}\approx1.9$ for Li. These temperatures and charge states correspond to three-body recombination rates of -2.52×10^{28} m^3/s^1 for Sn and -6.10×10^{23} m^{-3} s^{-1} for Li. These calculations have shown that the three-body recombination rate in Sn plasma is five orders higher, and hence, the out-of-band emission could be considerably higher in the case of an Sn plasma compared to a Li plasma. This will lead to broader atomic and ionic kinetic peaks from Sn plasma.

IV. SUMMARY

We have conducted a comprehensive comparison of EUV and visible emissions, and ion debris features, of Nd:YAG laser generated Sn and Li plasmas under identical experimental conditions. The CE of the EUV radiation has been shown to strongly depend on laser spot size, laser intensity, and target composition. The Sn plasma reached a peak CE of 2%, and Li CE peaked at 1%. The peak CE values obtained for Sn and Li have been found to be independent of spot size, though the two materials reach their peaks at different intensities. The laser intensity required for the optimal CE value was found to be inversely proportional to the laser spot size. The observed saturation or reduction in CE in plasmas at higher intensities could be due to opacity effects. EUV spectral studies of Sn and Li plasmas created by pulses of varying intensity were performed to characterize self-absorption. The EUV emission of Sn plasma showed a broad-band UTA emission concentrated around 13.5 nm, due to emissions from the Sn^{9+}–Sn^{13+} transitions. At high laser energies, a spectral dip at the UTA peak appears due to self-absorption. Li plasmas possess discrete line structures, primarily the Lyman-α line, which became more intense with increasing laser intensity without changing the spectral features. An EUV-filtered pinhole camera showed that the plasma plumes appear to take on different shapes but have similar aspect ratios.

FC analysis of Sn and Li plasma ion emission was used to generate ion and KE profiles. Li ions exhibit a much narrower kinetic profile than Sn ions but the less massive Li ions have a considerably lower KE than the Sn ions. The plasma ions undergo three-body recombination as they expanded toward the FC, which implied that Li atoms are less prone to recombination. Our calculations shown that the three-body recombination rate within the Sn plasma is five orders greater than those of Li plasmas. The maximum probable KEs and ion flux of Sn and Li plasmas depend on the laser intensity and display an exponentially saturating trend. Plasma shielding and/or absorption are likely responsible for the reduction in KEs and ion flux at higher laser intensities. Sn plasmas have been found to be more damaging to MLMs due to their higher peak KEs. The Li plasmas demonstrate greater ion fluence but their lower energies would allow an easier implementation of electromagnetic charged particle debris mitigation systems.

OES was employed to record time-integrated spectra showing a strong presence of energetic single ions and neutrals in Sn and Li plasmas. The expansion velocities estimated from optical TOF studies are in good agreement with the FC measurement values for Li ions but the Sn ion velocity is considerably lower than its FC measured value. This is because the Sn FC signal contains ≥13 distinct charge states, as opposed to the three ionic stages of Li. The observed KEs of Sn neutrals are more than 6× greater than those of Li but the energies of the neutrals are much less compared with the ion KEs.

[1] T. Ito and S. Okazaki, Nature (London) **406**, 1027 (2000).
[2] H. Sewell, A. Chen, J. Finders, and M. Dusa, Jpn. J. Appl. Phys. **48**, 06FA01 (2009).
[3] V. Bakshi, *EUV Sources for Lithography* (SPIE, New York, 2006).
[4] B. Wu and A. Kumar, J. Vac. Sci. Technol. B **25**, 1743 (2007).
[5] V. M. Borisov, A. V. Eltsov, A. S. Ivanov, Y. B. Kiryukhin, O. B. Khristoforov, V. A. Mishchenko, A. V. Prokofiev, A. Y. Vinokhodov, and V. A. Vodchits, J. Phys. D **37**, 3254 (2004).
[6] M. Masnavi, M. Nakajima, E. Hotta, and K. Horioka, J. Appl. Phys. **103**, 013303 (2008).
[7] W. T. Silfvast, IEEE J. Quantum Electron. **35**, 700 (1999).
[8] Y. Tao, M. S. Tillack, S. S. Harilal, K. L. Sequoia, and F. Najmabadi, J. Appl. Phys. **101**, 023305 (2007).
[9] S. S. Harilal, M. S. Tillack, B. O'Shay, Y. Tao, and A. Nikroo, Opt. Lett. **31**, 1549 (2006).
[10] N. Böwering, M. Martins, W. N. Partlo, and I. V. Fomenkov, J. Appl. Phys. **95**, 16 (2004).
[11] T. Higashiguchi, K. Kawasaki, W. Sasaki, and S. Kubodera, Appl. Phys. Lett. **88**, 161502 (2006).
[12] J. White, P. Dunne, P. Hayden, F. O'Reilly, and G. O'Sullivan, Appl. Phys. Lett. **90**, 181502 (2007).
[13] T. Ando, S. Fujioka, H. Nishimura, N. Ueda, Y. Yasuda, K. Nagai, T. Norimatsu, M. Murakami, K. Nishihara, N. Miyanaga, Y. Izawa, K. Mima, and A. Sunahara, Appl. Phys. Lett. **89**, 151501 (2006).
[14] Y. Tao, S. S. Harilal, M. S. Tillack, B. O'Shay, and F. Najmabadi, Opt. Lett. **31**, 2492 (2006).
[15] S. S. Harilal, B. O'Shay, M. S. Tillack, and Y. Tao, J. Phys. D **39**, 484 (2006).
[16] A. Hassanein, V. Sizyuk, T. Sizyuk, and S. S. Harilal, J. Micro/Nanolith. MEMS MOEMS **8**, 041503 (2009).
[17] P. Hayden, A. Cummings, N. Murphy, G. O'Sullivan, P. Sheridan, J. White, and P. Dunne, J. Appl. Phys. **99**, 093302 (2006).
[18] A. Nagano, T. Inoue, P. E. Nica, S. Amano, S. Miyamoto, and T. Mochizuki, Appl. Phys. Lett. **90**, 151502 (2007).
[19] S. S. Harilal, B. O'Shay, Y. Tao, and M. S. Tillack, Appl. Phys. B: Lasers Opt. **86**, 547 (2007).
[20] M. J. Neumann, M. Cruce, P. Brown, S. N. Srivasta, D. N. Ruzic, and O. Khodykin, Proc. SPIE **6517**, Y5172 (2007).
[21] M. Shimomura, S. Fujioka, T. Ando, H. Sakaguchi, Y. Nakai, Y. Yasuda, H. Nishimura, K. Nagai, T. Norimatsu, K. Nishihara, N. Miyanaga, Y. Izawa, and K. Mima, Appl. Phys. Express **1**, 056001 (2008).
[22] H. Tanaka, Y. Hashimoto, K. Tamaru, A. Takahashi, and T. Okada, Appl. Phys. Lett. **89**, 181109 (2006).
[23] J. P. Allain, M. Neito, M. R. Hendricks, P. Plotkin, S. S. Harilal, and A.

Hassanein, Rev. Sci. Instrum. **78**, 113105 (2007).
[24]S. Bollanti, F. Bonfigli, E. Burattini, P. Di Lazzaro, F. Flora, A. Grilli, T. Letardi, N. Lisi, A. Marinai, L. Mezi, D. Murra, and C. Zheng, Appl. Phys. B: Lasers Opt. **76**, 277 (2003).
[25]Y. Ueno, G. Soumagne, A. Sumitani, A. Endo, T. Higashiguchi, and N. Yugami, Appl. Phys. Lett. **92**, 211503 (2008).
[26]S. A. George, W. T. Silfvast, K. Takenoshita, R. T. Bernath, C. S. Koay, G. Shimkaveg, and M. C. Richardson, Opt. Lett. **32**, 997 (2007).
[27]O. Morris, P. Hayden, F. O'Reilly, N. Murphy, P. Dunne, and V. Bakshi, Appl. Phys. Lett. **91**, 081506 (2007).
[28]T. Okuno, S. Fujioka, H. Nishimura, Y. Tao, K. Nagai, Q. Gu, N. Ueda, T. Ando, K. Nishihara, T. Norimatsu, N. Miyanaga, Y. Izawa, K. Mima, A. Sunahara, H. Furukawa, and A. Sasaki, Appl. Phys. Lett. **88**, 161501 (2006).
[29]S. S. Harilal, J. Appl. Phys. **102**, 123306 (2007).
[30]S. Fujioka, H. Nishimura, K. Nishihara, A. Sasaki, A. Sunahara, T. Okuno, N. Ueda, T. Ando, Y. Tao, Y. Shimada, K. Hashimoto, M. Yamaura, K. Shigemori, M. Nakai, K. Nagai, T. Norimatsu, T. Nishikawa, N. Miyanaga, Y. Izawa, and K. Mima, Phys. Rev. Lett. **95**, 235004 (2005).
[31]J. White, A. Cummings, P. Dunne, P. Hayden, and G. O'Sullivan, J. Appl. Phys. **101**, 043301 (2007).
[32]S. Bollanti, P. Di Lazzaro, F. Flora, L. Mezi, D. Murra, and A. Torre, Appl. Phys. B: Lasers Opt. **96**, 479 (2009).
[33]V. Sizyuk and A. Hassanein. J. Micro/Nanolith. MEMS MOEMS **6**, 043003 (2007).
[34]R. Janmohamed, G. Redman, and Y. Y. Tsui, IEEE Trans. Plasma Sci. **34**, 455 (2006).
[35]J. White, P. Dunne, P. Hayden, and G. O'Sullivan, J. Appl. Phys. **106**, 113303 (2009).
[36]S. S. Harilal, R. C. Issac, C. V. Bindhu, V. P. N. Nampoori, and C. P. G. Vallabhan, J. Appl. Phys. **80**, 3561 (1996).
[37]K. Takenoshita, C. S. Koay, S. Teerawattansook, M. Richardson, and V. Bakshi, in *Emerging Lithographic Technologies IX: Pts. 1 and 2*, edited by R. S. Mackay (SPIE, Bellingham, 2005), Vol. 5751, p. 563.
[38]D. Nakamura, T. Akiyama, A. Takahashi, and T. Okada, J. Laser Micro/Nanoeng. **3**, 196 (2008).
[39]S. S. Harilal, C. V. Bindhu, M. S. Tillack, F. Najmabadi, and A. C. Gaeris, J. Phys. D **35**, 2935 (2002).
[40]S. S. Harilal, C. V. Bindhu, M. S. Tillack, F. Najmabadi, and A. C. Gaeris, J. Appl. Phys. **93**, 2380 (2003).
[41]S. S. Harilal, Appl. Opt. **43**, 3931 (2004).
[42]R. A. Burdt, S. Yuspeh, K. L. Sequoia, Y. Z. Tao, M. S. Tillack, and F. Najmabadi, J. Appl. Phys. **106**, 033310 (2009).
[43]P. T. Rumsby and J. W. M. Paul, Plasma Phys. **16**, 247 (1974).
[44]D. Campos, S. S. Harilal, and A. Hassanein, Appl. Phys. Lett. **96**, 151501 (2010).